Electronic Supplementary Information

Revealing the Origin of Voltage Loss in Mixed-Halide Perovskite Solar Cells

Suhas Mahesh[a], James M. Ball[a], Robert D. J. Oliver[a], David P. McMeekin[b], Pabitra K. Nayak*[a], Michael. B. Johnston[a] and Henry J. Snaith*[a]

a. *Clarendon Laboratory, University of Oxford, Parks Road, Oxford OX1 3PU, UK.*

b. *Department of Chemical Engineering, Monash University, Clayton, Victoria 3800*

Email: pabitra.nayak@physics.ox.ac.uk, henry.snaith@physics.ox.ac.uk

Preparation of $FA_{0.83}Cs_{0.17}Pb(I_xBr_{1-x})_3$ based Solar cells

In this work, all powders were used as purchased without further purification and weighed in a nitrogen filled glovebox. To form the perovskite precursor, lead iodide (PbI_2, 99.99 %, Alfa-Aesar), lead bromide ($PbBr_2$, >98 %, Alfa-Aesar), cesium iodide (CsI, 99.99%, Alfa-Aesar), and formamidinium iodide (FAI, GreatCell Solar) were weighed stoichiometrically to the target perovskite composition (e.g. $FA_{0.83}Cs_{0.17}Pb(I_{0.6}Br_{0.4})_3$). To form the precursor solution, a 4:1 volume ratio of anhydrous N,N-dimethylformamide (DMF, Sigma Aldrich)) and anhydrous dimethyl sulfoxide (DMSO, (Sigma Aldrich) was added to achieve a concentration of 1.4 M.

Poly(4-butylphenyl-diphenyl-amine) (polyTPD, 1-Material) was used as hole transporting material (HTM). Poly-TPD was dissolved in toluene at a concentration of 1 mg/mL and was doped with 20 wt% 2,3,5,6-Tetrafluoro-7,7,8,8-tetracyanoquinodimethane (F4-TCNQ, Lumtec). [6,6]-phenyl-C_{61}-butyric acid methyl ester ($PC_{61}BM$, >99.5%, Solenne BV) was used as the electron transporting material (ETM). PCBM was dissolved in a volume ratio of 3:1 chlorobenzene: 1,2-dichlorobenzene and used at a concentration of 20 mg/mL. Bathocuproine (BCP, 98 %, Alfa-Aesar) was implemented as a hole blocking layer (HBL) at concentration of 0.5 mg/mL in isopropanol (IPA).

The p-i-n device architecture employed for the FACs cells was FTO/polyTPD/perovskite/PCBM/BCP/Ag.

Fluorine-doped tin oxide (FTO, Pilkington TEC 7, 7 Ω/sq. sheet resistivity) was used as the transparent electrode. Zinc powder and 2 M HCl were used to etch the FTO to the desired electrode pattern. The substrates were then cleaned by sonication in deionised (DI) water with 1 vol% Decon90 cleaning detergent, before being rinsed with DI water, acetone and IPA sequentially. The substrates were then dried with a nitrogen gun followed by an UV-Ozone treatment for 15 minutes, prior to use.

Immediately after the substrate preparation was complete, the HTM was deposited in ambient air. 70 µL of the doped polyTPD solution was dispensed onto a substrate spinning at 2000 rpm for 20 seconds, and then annealed at 130 °C for 10 minutes. Then the perovskite layer was deposited in a nitrogen filled glovebox. 170 µL of the perovskite precursor solution was dispensed onto a substrate spinning at 1000 rpm. After 5 seconds, the substrate was accelerated to 5000 rpm over the course of 5 s and remained at this speed for 30 s. 5 s before the end of this process, 350 µL of anisole was applied to the spinning substrate as an anti-solvent quench. The films were then annealed at 100 °C for 45 minutes.

The ETM and HBL were both deposited in a nitrogen filled glovebox. 40 µL of the PCBM solution was dynamically spun onto the perovskite layer at 2000 rpm for 20 s, then heated at 100 °C for 3 mins to remove any remaining solvent. BCP was applied on the PCBM layer by depositing 100 µL onto a substrate spinning at 5000 rpm for 30 s before being heated to 100 °C for one minute to remove any remaining solvent.

Devices were completed by thermally evaporating silver electrodes (100 nm) through shadow masks (active area defined as 0.0919 cm^2) under high vacuum (~10^{-6} mbar) using a Nano36, Kurt J. Lesker thermal evaporator.

Preparation of $FA_{0.83}MA_{0.17}Pb(I_{0.4}Br_{0.6})_3$ based Solar Cells

The structure of the cell was: FTO/SnO_2/Perovskite/Spiro-OMeTAD/Au. The SnO_2 and Spiro-OMeTAD layers were deposited as described by us elsewhere [1,2]. FAI (Dyesol), MABr (Dyesol), PbI_2 (TCL Chemicals) and $PbBr_2$ (Alfa Aesar) were weighed to exact stoichiometry in a glovebox and dissolved in 4:1 DMF:DMSO (Sigma Aldrich), such that the overall concentration was 0.5 M. The solution was stirred at 85°C for 5 hours in nitrogen. All solution processing and annealing was done in a nitrogen filled glovebox. The perovskite was spun in on top of the SnO_2 at 1000 rpm for 10 s, followed by 6000 rpm for 35 s. The film was quenched with 150 uL of Anisol, 40 s into the spin. The film was annealed at 100°C for 1 hour in the glovebox. 2 nm of Cr, followed by 100 nm of Au was evaporated on top of the HTL using a Nano36, Kurt.K.Lesker thermal evaporator held under high vacuum (~10^{-6} mbar). The device active area was 0.0919cm^2.

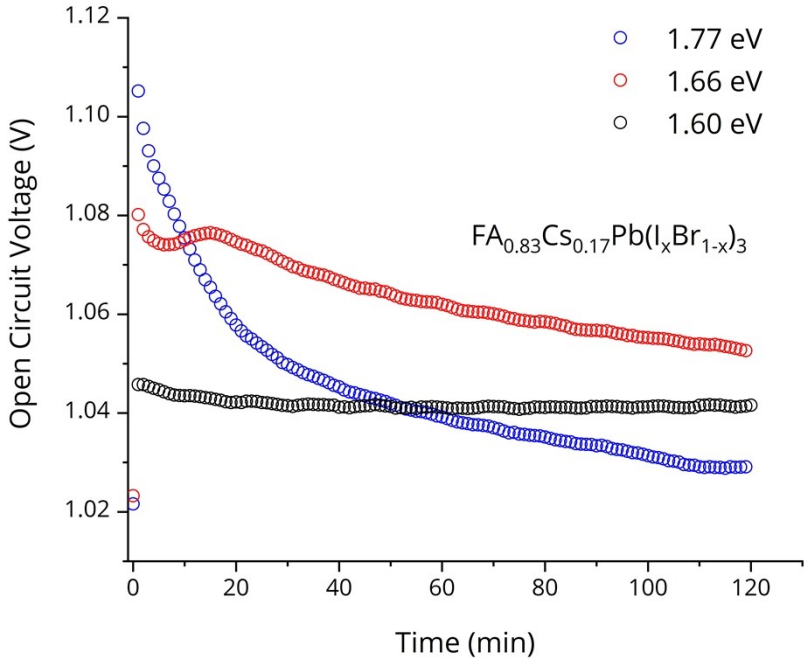

Fig. S1. Time-evolution of V_{oc} for FACs based p-i-n solar cells, tracked at the same time as the Fourier Transform Photocurrent Spectroscopy (FTPS)

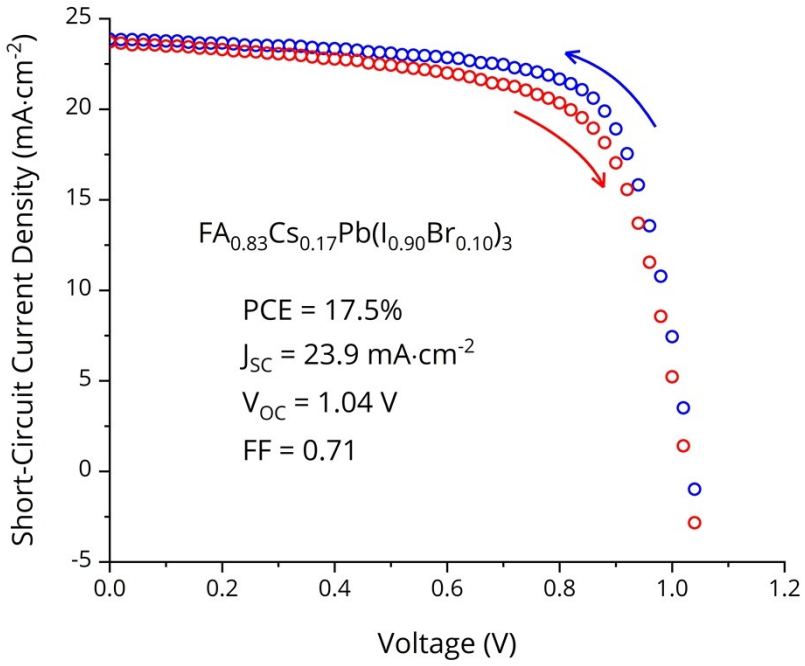

Fig. S2. JV characteristics of the $FA_{0.83}Cs_{0.17}Pb(I_{0.90}Br_{0.10})_3$ device measured under simulated AM1.5 illumination.

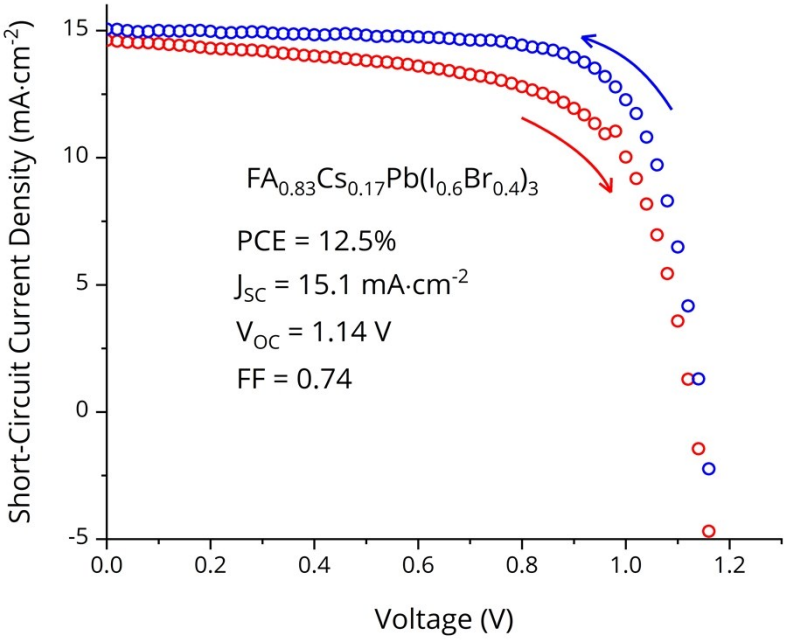

Fig. S3. JV characteristics of the $FA_{0.83}Cs_{0.17}Pb(I_{0.60}Br_{0.40})_3$ device measured under simulated AM1.5 illumination.

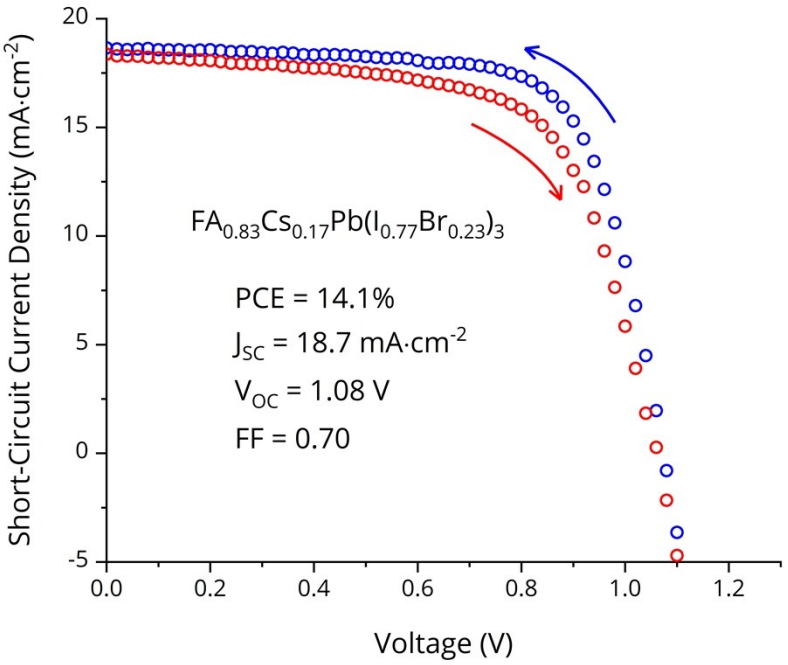

Fig. S4. JV characteristics of the $FA_{0.83}Cs_{0.17}Pb(I_{0.77}Br_{0.23})_3$ device measured under simulated AM1.5 illumination.

Fourier Transform Photocurrent Spectroscopy (FTPS) Setup and Measurement

Fourier-transform photocurrent spectroscopy was used to measure the photovoltaic external quantum efficiency (EQE_{PV}) of solar cells using a Bruker Vertex 80 Fourier-transform infrared spectrometer. A Newport Orial Sol3A solar simulator was used to provide a simulated AM1.5G illumination spectrum. The cells were illuminated with this light source to induce halide segregation but measurements were performed with an optical filter to enable enhanced dynamic range in the sub-bandgap region. The current signal from the solar cell was converted to a voltage using a Stanford Research SR570 current preamplifier and fed into the spectrometer analog-to-digital converter for measurement. The absolute values of EQE_{PV} were calculated based on the ratio of the current from the cell to that of the current from a calibrated Si reference solar cell (Newport) of known EQE_{PV}

Effective Medium Approximation

The approach of Hoerantner et al.[3] in shifting the optical constants of $MAPbI_3$[4] was followed to simulate the optical constants of the iodide-bromide mixed halide perovskites. An 18mV Urbach tail was also appended. Since the trend in V_{OC} is our main focus and the V_{OC} is determined largely by the absorption tail, this approach is sufficient for the purpose. To model the expected loss from a two-phase segregation (Fig 1c, 1d), the complex refractive index of the halide-segregated film was modelled as a Bruggeman effective medium of the two phases using the implementation in the free program Optical[5]. Since the amount of minority phase is small, the Bruggeman effective refractive index turns out to be very close to a linear combination of the two refractive indices.

Optical Modelling

The optical modelling was done using a modified version of the implementation of the generalised transfer matrix method developed by E. Centurioni[5]. All calculations were done in Python using the libraries NumPy and SciPy. The model takes the wavelength dependant complex refractive index, the layer thicknesses and the incident angle (normal incidence in our case) as input. It calculates the absorptance of each layer, and the transmittance and the reflectance of the stack. To model the EQE_{PV} of the halide-segregated perovskite cell, we used a hypothetical stack: FTO (200nm)/SnO_2 (10nm)/Perovskite (400nm)/Spiro-OMeTAD (200nm)/Ag (100nm). We assume 100% collection efficiency and thus take the EQE_{PV} to be the same as the absorptance of the perovskite. This assumption does not dictate our results, since V_{oc} is only weakly dependant on the current. The complex refractive index of the perovskite was got via the effective medium approximation, as described above. For FTO[6], SnO_2[7], Spiro-OMeTAD[8] and Ag[9], values reported in the literature were used.

Detailed Balance Calculations

The open-circuit voltage was calculated using the equation[10]:

$$V_{oc} = \frac{kT}{q} \ln\left(\frac{J_{sc}}{J_0}\right) \#(1)$$

J_{sc} is the overlap integral of the solar AM1.5 spectrum with the EQE_{PV} of the cell. Similarly, J_0 is calculated as the overlap integral of the Blackbody spectrum at 300K with the EQE_{PV} of the cell:

$$J_{sc} = q\int_0^\infty EQE_{PV}(\lambda) \cdot \phi_{AM1.5}(\lambda) \cdot d\lambda \#(2)$$

$$J_0 = \frac{J_{0,rad}}{EQE_{EL}} = \frac{q}{EQE_{EL}}\int_0^\infty \phi_{BB}(\lambda) \cdot EQE_{PV}(\lambda) \cdot d\lambda \#(3)$$

Here, the EQE_{EL} is the electroluminescence quantum efficiency.

Effect of EQE_{EL}

To investigate the effect of different EQE_{EL} of the majority and minority phases, we sum dark current contributions from the minority and majority phases. The dark current contribution from the majority phase is calculated by integrating over the unsegregated device EQE_{PV} (Equation 4). The dark current contribution from the minority phase, is calculated by integrating over the segregated EQE_{PV}, after subtracting the unsegregated EQE_{PV} (Equation 5). For simplicity, the broadening in the majority phase is considered to be part of the minority phase.

$$J_{0,maj} = \frac{q}{EQE_{EL,maj}}\int_0^\infty \phi_{BB}(\lambda) \cdot EQE_{PV,unseg}(\lambda) \cdot d\lambda \#(4)$$

$$J_{0,min} = \frac{q}{EQE_{EL,min}}\int_0^\infty \phi_{BB}(\lambda) \cdot (EQE_{PV,seg}(\lambda) - EQE_{PV,unseg}(\lambda)) \cdot d\lambda \#(5)$$

Distribution of Bandgaps Calculation

We model the perovskite as being made of two components:

1. A majority phase: A phase mixture comprising of exponentially distributed bandgaps.
2. A minority phase: phase pure, i.e. a Dirac-delta bandgap distribution.

The optical constants of the perovskite are modelled through a linear effective medium approximation. The optical constants of perovskites of different bandgaps are approximated by linearly shifting the absorption edge and then performing a Kramers-Kronig transform to obtain the refractive index in the same fashion as Hoerantner et al[11]. Work by McMeekin et al. demonstrates that the bandgaps of mixed-halide perovskites do shift linearly in this way[2]

$$\tilde{n_{EMA,maj}} = \int \tilde{n}(E) \cdot f(E) \cdot dE$$

Here $f(E) \cdot dE$ is the molar fraction of the film with bandgap at E. We have verified that, in this case, the linear approximation nearly coincides with the more specialised Bruggeman effective medium approximation. In our case, the distribution $f(E)$ is taken to be exponential:

$$f(E) = \begin{cases} \alpha e^{\alpha(E - E_g)}, & E < E_g \\ 0, & E > E_g \end{cases}$$

As we have already mentioned, the minority phase is modelled as a pure phase.

The segregated film refractive index is calculated using Bruggeman EMA, assuming fractions x and $1 - x$ for the two phases respectively:

$$n_{EMA} = EMA(n_{EMA,maj}, n_{min})$$

The effective refractive index is used to optically model the absorptance of the perovskite layer, which is used to fit the measured EQE_{PV} of the segregated perovskite, by varying the parameters x and α.

References

1 M. L. Petrus, K. Schutt, M. T. Sirtl, E. M. Hutter, A. C. Closs, J. M. Ball, J. C. Bijleveld, A. Petrozza, T. Bein, T. J. Dingemans, T. J. Savenije, H. Snaith and P. Docampo, *Adv. Energy Mater.*, 2018, **8**, 1801605.

2 D. P. McMeekin, G. Sadoughi, W. Rehman, G. E. Eperon, M. Saliba, M. T. Horantner, A.

Haghighirad, N. Sakai, L. Korte, B. Rech, M. B. Johnston, L. M. Herz and H. J. Snaith, *Science*, 2016, **351**, 151–155.

3 M. T. Hörantner and H. J. Snaith, *Energy Environ. Sci.*, 2017, **10**, 1983–1993.

4 P. Löper, M. Stuckelberger, B. Niesen, J. Werner, M. Filipič, S.-J. Moon, J.-H. Yum, M. Topič, S. De Wolf and C. Ballif, *J. Phys. Chem. Lett.*, 2015, **6**, 66–71.

5 E. Centurioni, *Appl. Opt.*, 2005, **44**, 7532.

6 J. M. Ball, S. D. Stranks, M. T. Hörantner, S. Hüttner, W. Zhang, E. J. W. Crossland, I. Ramirez, M. Riede, M. B. Johnston, R. H. Friend and H. J. Snaith, *Energy Environ. Sci.*, 2015, **8**, 602–609.

7 E. Çetinörgü, C. Gümüs, S. Goldsmith and F. Mansur, *Phys. Status Solidi Appl. Mater. Sci.*, 2007, **204**, 3278–3285.

8 M. Filipič, P. Löper, B. Niesen, S. De Wolf, J. Krč, C. Ballif and M. Topič, *Opt. Express*, 2015, **23**, A263--A278.

9 P. B. Johnson and R. W. Christy, *Phys. Rev. B*, 1972, **6**, 4370–4379.

10 K. Tvingstedt, O. Malinkiewicz, A. Baumann, C. Deibel, H. J. Snaith, V. Dyakonov and H. J. Bolink, *Sci. Rep.*, 2014, **4**, 1–7.

11 M. T. Hörantner, T. Leijtens, M. E. Ziffer, G. E. Eperon, M. G. Christoforo, M. D. McGehee and H. J. Snaith, *ACS Energy Lett.*, 2017, **2**, 2506–2513.